Geoscience Frontiers 9 (2018) 1609–1618

HOSTED BY

Contents lists available at ScienceDirect

China University of Geosciences (Beijing)

Geoscience Frontiers

journal homepage: www.elsevier.com/locate/gsf

Research Paper

Random field characterization of uniaxial compressive strength and elastic modulus for intact rocks

Huaxin Liu, Xiaohui Qi*

School of Civil and Environmental Engineering, Nanyang Technological University, Block N1, 50 Nanyang Avenue, Singapore 639798, Singapore

ARTICLE INFO

Article history:
Received 21 June 2017
Received in revised form
7 September 2017
Accepted 3 November 2017
Available online 18 December 2017

Keywords:
Uniaxial compressive strength
Elastic modulus
Scale of fluctuation
Autocorrelation function
Spatial variability
Bayesian approach

ABSTRACT

Rock properties exhibit spatial variabilities due to complex geological processes such as sedimentation, metamorphism, weathering, and tectogenesis. Although recognized as an important factor controlling the safety of geotechnical structures in rock engineering, the spatial variability of rock properties is rarely quantified. Hence, this study characterizes the autocorrelation structures and scales of fluctuation of two important parameters of intact rocks, i.e. uniaxial compressive strength (UCS) and elastic modulus (EM). UCS and EM data for sedimentary and igneous rocks are collected. The autocorrelation structures are selected using a Bayesian model class selection approach and the scales of fluctuation for these two parameters are estimated using a Bayesian updating method. The results show that the autocorrelation structures for UCS and EM could be best described by a single exponential autocorrelation function. The scales of fluctuation for UCS and EM respectively range from 0.3 m to 8.0 m and from 0.3 m to 8.4 m. These results serve as guidelines for selecting proper autocorrelation functions and autocorrelation distances for rock properties in reliability analyses and could also be used as prior information for quantifying the spatial variability of rock properties in a Bayesian framework.

1. Introduction

During formation, rocks undergo complex geological processes such as sedimentation, metamorphism, weathering, and tectogenesis. Therefore, they exhibit inherent variabilities, which are a major source of uncertainties associated with rock properties (Dasaka and Zhang, 2012; Zhu and Zhang, 2013; Aladejare and Wang, 2017). In literature, most reliability evaluations of rock engineering problems treated the rock properties as random variables (e.g. Li and Low, 2010; Lü and Low, 2011; Lü et al., 2011, 2013; Zhang and Goh, 2013, 2014, 2016; Goh et al., 2017; Liu and Low, 2017). However, due to the inherent uncertainty, it is more realistic to model the rock property as a random field than a random variable. The inherent variability of rock properties should be considered in designs and reliability analyses of geotechnical structures.

In designs and reliability evaluations of rock engineering problems, one of the most important input parameters is the scale of fluctuation or autocorrelation distance, which provides an indication of the distance within which the properties show relatively strong autocorrelation (Phoon and Kulhawy, 1999; Li et al., 2014, 2015a,b; Liu et al., 2015, 2017a). However, most of the existing studies conducted the reliability analysis based on assumed scales of fluctuation of rock properties rather than values inferred from real rock data (e.g. Gravanis et al., 2014). Clearly, there lacks a guideline on selecting a reasonable value or a range of scales of fluctuation for rock properties. Apart from the scale of fluctuation, the autocorrelation structure is another significant feature that affects the modeling of spatial variabilities of rock properties. The autocorrelation structure describes how the autocorrelation coefficient of a geotechnical property varies with the separation distance between two points (Phoon et al., 2003; Liu et al., 2017b). In geotechnical practice, more than one autocorrelation function is commonly used to characterize the autocorrelation structure of geotechnical properties. Li et al. (2015b) and Liu et al. (2017c) showed that different autocorrelation structures of geotechnical properties may lead to different reliabilities of geotechnical structures. However, to the best of our knowledge, there rarely exist any studies quantifying the scale of fluctuation and autocorrelation structure of rock properties. As commented by Hsu and Nelson (2006) and Phoon and Retief (2016), very little work had been done on characterizing the spatial variability of rock properties. One of the possible reasons is that the extraction of rock samples is

* Corresponding author.
E-mail address: qixiaohui@ntu.edu.sg (X. Qi).
Peer-review under responsibility of China University of Geosciences (Beijing).

https://doi.org/10.1016/j.gsf.2017.11.014

difficult and costly, and testing of rock properties always requires very complicated equipment, resulting in very sparse rock data (Aladejare and Wang, 2017). Nevertheless, this sparsity should not downgrade the significance of spatial variability characterization of rock properties, even though the characterization might be a rough one. Indeed, the results of spatial variability characterization of geotechnical properties may also serve as a prior information in Bayesian updating (e.g. Aladejare and Wang, 2017) and are helpful to design effective site investigation schemes (e.g. Jaksa et al., 2005; Gong et al., 2017).

In view of the limited studies on the spatial variability characterization of rock properties, this paper evaluates the most suitable autocorrelation structures and quantifies the scales of fluctuation for two important parameters of intact rocks, i.e. the uniaxial compressive strength (UCS) and elastic modulus (EM). UCS and EM data for the igneous rock and sedimentary rock from different areas are collected. These two parameters for the intact rock are selected because UCS is one of the most widely used indicators of the rock strength and is critical in determining the Hoek-Brown failure criterion parameters (Hoek et al., 2002) and EM of the intact rock is critical in estimating the EM of the rock mass (Hoek and Diederichs, 2006). A Bayesian model class selection approach is used to select the most suitable autocorrelation function for UCS and EM because the approach is able to select the most plausible model with a high fitting capacity as well as a high robustness (e.g. Cao and Wang, 2013, 2014; Wang and Aladejare, 2015). The scales of fluctuation for UCS and EM are subsequently quantified using a Bayesian updating method. The autocorrelation coefficients for different autocorrelation functions are compared. The results provide a guideline for selecting reasonable autocorrelation functions and scales of fluctuation for UCS and EM of intact rocks.

2. Random field modeling of spatial variability for UCS and EM of rocks

The spatial variabilities of UCS and EM of rocks are modeled by random fields. Lognormal distributions are selected to describe the probabilistic distribution of the two parameters to avoid negative values. Suppose a lognormally distributed random field $Y(z)$ (z is the depth below the ground surface) with the mean given by a linear trend function in Eq. (1) and a constant standard deviation, σ.

$$t(z) = az + b \tag{1}$$

where $t(z)$ is the mean trend; a and b are two regression coefficients. It can be easily deduced that the logarithm of $Y(z)$, $\ln(Y(z))$, is a normally distributed random field with the mean, $\mu_N(z)$ and standard deviation, $\sigma_N(z)$ given by Eq. (2) (Li et al., 2014).

$$\begin{cases} \mu_N(z) = \ln(t(z)) - 0.5\ln\left(1+\left(\dfrac{\sigma}{t(z)}\right)^2\right) \\ \sigma_N(z) = \sqrt{\ln\left(1+\left(\dfrac{\sigma}{t(z)}\right)^2\right)} \end{cases} \tag{2}$$

Note that $\mu_N(z)$ and $\sigma_N(z)$ vary with depth if $Y(z)$ has an inconstant trend, i.e. $a \neq 0$.

The autocorrelation structure of a random field is usually represented by an autocorrelation function (e.g. Liu et al., 2014). Five autocorrelation functions commonly used in geotechnical practice (see Eq. (3)) are considered in this study, i.e. single exponential autocorrelation function (SEACF), Gaussian autocorrelation function (GACF), binary noise autocorrelation function (BNACF), second-order Markov autocorrelation function (SMACF) and cosine exponential autocorrelation function (CEACF) (Phoon et al., 2003). These

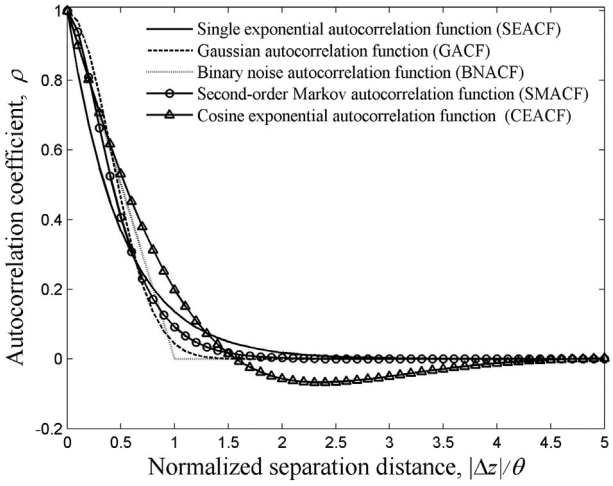

Figure 1. Five autocorrelation functions commonly used in geotechnical practice.

five autocorrelation functions are respectively termed M_1, M_2, …, and M_5.

$$\text{SEACF}(M_1): \rho(\Delta z) = \exp\left(-\frac{2|\Delta z|}{\theta}\right) \tag{3a}$$

$$\text{GACF}(M_2): \rho(\Delta z) = \exp\left[-\pi\left(\frac{\Delta z}{\theta}\right)^2\right] \tag{3b}$$

$$\text{BNACF}(M_3): \rho(\Delta z) = \begin{cases} 1-\dfrac{|\Delta z|}{\theta} & \text{for } |\Delta z| \le \theta \\ 0 & \text{otherwise} \end{cases} \tag{3c}$$

$$\text{SMACF}(M_4): \rho(\Delta z) = \left(1+4\frac{|\Delta z|}{\theta}\right)\exp\left(-\frac{4|\Delta z|}{\theta}\right) \tag{3d}$$

$$\text{CEACF}(M_5): \rho(\Delta z) = \exp\left(-\frac{|\Delta z|}{\theta}\right)\cos\left(\frac{\Delta z}{\theta}\right) \tag{3e}$$

where $\rho(\Delta z) = \rho(z_i - z_j)$ is the autocorrelation coefficient between two standard normally distributed random variables $[\ln(Y(z_i)) - \mu_N(z_i)]/\sigma_N(z_i)$ and $[\ln(Y(z_j)) - \mu_N(z_j)]/\sigma_N(z_j)$; z_j and z_j are vertical coordinates of the two points associated with $Y(z_i)$ and $Y(z_j)$; θ is the scale of fluctuation (SoF) in the vertical direction. The autocorrelation coefficients for the five autocorrelation functions are plotted in Fig. 1. With Eq. (3), it is easy to evaluate the autocorrelation matrix, $\mathbf{R}^{\mathbf{M_i}}$, for a random vector $[\xi(z_1), \xi(z_2), \cdots, \xi(z_n)]$, where $\xi(z_k) = [\ln(Y(z_k)) - \mu_N(z_k)]/\sigma_N(z_k)$. The (k, l)th entry of R^{M_i}, $R_{kl}^{M_i}$ represents the autocorrelation coefficient between $\xi(z_k)$ and $\xi(z_l)$ and for the autocorrelation model M_i. $R_{kl}^{M_i}$ is equal to $\rho(z_k - z_l)$ evaluated from the corresponding autocorrelation function in Eq. (3). Furthermore, the covariance matrix, $\mathbf{C}^{\mathbf{M_i}}$, for the random vector $[\ln(Y(z_1)), \ln(Y(z_2)), \ldots, \ln(Y(z_n))]$ can be obtained based on the relation between covariance and correlation coefficient. The (k, l)th entry of $\mathbf{C}^{\mathbf{M_i}}$, $C_{kl}^{M_i}$ represents the covariance between $\ln(Y(z_k))$ and $\ln(Y(z_l))$, and is given by Eq. (4).

$$C_{kl}^{M_i} = R_{kl}^{M_i}\sigma_N(z_k)\sigma_N(z_l) \tag{4}$$

where $\sigma_N(z_k)$ and $\sigma_N(z_l)$ respectively are the standard deviations of $\ln(Y(z_k))$ and $\ln(Y(z_l))$, and are evaluated through Eq. (2).

Let $\widehat{\mathbf{Y}} = [\widehat{Y}(z_1), \widehat{Y}(z_2), \cdots, \widehat{Y}(z_n)]^T$ be a set of observations of Y at depth $[z_1, z_2, \cdots, z_n]^T$. Based on the definition of multivariate normal distribution, the likelihood of the observations conditional on the random field parameters a, b, σ, and θ, and autocorrelation function M_i is given by Eq. (5).

$$p\left(\widehat{\mathbf{Y}}|a,b,\sigma,\theta;M_i\right) = \frac{\exp\left[-\frac{1}{2}\left(\ln\left(\widehat{\mathbf{Y}}\right)-\boldsymbol{\mu}_{\mathbf{N},\mathbf{n}}\right)^T\left(\mathbf{C}^{\mathbf{M_i}}\right)^{-1}\left(\ln\left(\widehat{\mathbf{Y}}\right)-\boldsymbol{\mu}_{\mathbf{N},\mathbf{n}}\right)\right]}{\sqrt{(2\pi)^n|\mathbf{C}^{\mathbf{M_i}}|}} \tag{5}$$

where $|\mathbf{C}^{\mathbf{M_i}}|$ is the determinant of $\mathbf{C}^{\mathbf{M_i}}$; and $\boldsymbol{\mu}_{\mathbf{N},\mathbf{n}}$ is the mean of the random vector $[\ln(Y(z_1)), \ln(Y(z_2)), \cdots, \ln(Y(z_n))]^T$, which is evaluated through Eq. (2).

3. Bayesian model class selection and Bayesian updating approach

The Bayesian method has been successfully applied to the soil properties for probabilistic characterization of geotechnical parameters and model class selections. For example, Wang et al. (2010) characterized the uncertainty of sand friction angles using a Bayesian framework. Yuen (2010b) summarized the recent developments of Bayesian model class selection and its applications in civil engineering. Cao and Wang (2014) used the Bayesian model selection method to select the optimal spatial correlation function for soil parameters. Ching et al. (2015) compared the performances of the frequentist and Bayesian approaches in quantifying the statistical uncertainty of soil parameters. Tian et al. (2016) characterized the spatial variability of the friction angle using the cone penetration test data and Bayesian approach. However, the spatial variability of rock properties is seldom characterized. In this study, the Bayesian approach is used to select the optimal autocorrelation functions for UCS and EM and estimate the autocorrelation distances for these two parameters.

3.1. Selection of the most plausible autocorrelation function using Bayesian model class selection method

Since more than one autocorrelation function could be used to represent the autocorrelation structure of UCS and EM, it is of interest to evaluate which function is the most suitable one. The Bayesian model class selection approach is a well-known model selection method which is capable of finding out the optimal model with a high fitting capacity as well as good robustness. Herein the robustness means that the model has a low prediction error even in the presence of model errors and measurement noises. The approach is widely used to select models in geotechnical engineering (e.g. Cao and Wang, 2013, 2014; Wang and Aladejare, 2015). This Bayesian model selection approach is also used in this study to select the best autocorrelation functions of UCS and EM for rocks.

In the framework of Bayesian model class selection, the plausibility of a given model is measured by the probability of a class of model conditioned on given data. Suppose there are N_{ACF} ($N_{\mathrm{ACF}} = 5$ in this study) autocorrelation models, $M_1, M_2, \cdots, M_{N_{\mathrm{ACF}}}$. Based on the Bayesian theorem, the probability of each model conditional on the measured data $\widehat{\mathbf{Y}}$ is given by Eq. (6).

$$P\left(M_i|\widehat{\mathbf{Y}}\right) = \frac{P\left(\widehat{\mathbf{Y}}|M_i\right)P(M_i)}{P\left(\widehat{\mathbf{Y}}\right)} \tag{6}$$

where $P(\widehat{\mathbf{Y}})$ is the probability of the occurrence of $\widehat{\mathbf{Y}}$ and it is a normalizing constant independent of M_i; $P(\widehat{\mathbf{Y}}|M_i)$ is the evidence for the model class M_i provided by the data $\widehat{\mathbf{Y}}$, which expresses the likelihood of the data if the model class M_i is assumed; and $P(M_i)$ is the prior plausibility of the model class M_i, which reflects the user's judgment on the initial plausibility of the model M_i. The sum of the prior plausibility should be equal to 1 (Yuen, 2010a). In the case that the users have no clear information of the models' prior plausibility, the $P(M_i)$ is commonly set to be $1/N_{\mathrm{ACF}}$, i.e. the prior plausibility for various candidate models being equal. For this case, the plausibilities of the models are determined solely by the evidence. The model class with the maximum evidence is viewed to be the most suitable model.

Based on the law of total probability, the evidence for M_i provided by the data $\widehat{\mathbf{Y}}$ could be expressed by Eq. (7).

$$P\left(\widehat{\mathbf{Y}}|M_i\right) = \int_{\Theta_i} p\left(\widehat{\mathbf{Y}}|a,b,\sigma,\theta;M_i\right)p(a,b,\sigma,\theta|M_i)\mathrm{d}a\mathrm{d}b\mathrm{d}\sigma\mathrm{d}\theta \tag{7}$$

where Θ_i is the parameter space of the parameter vector $[a,b,\sigma,\theta]$, and $p(a,\ b,\ \sigma,\ \theta|M_i)$ is the prior probability density function (PDF) of the parameter vector $[a,b,\sigma,\theta]$. $p(a,\ b,\ \sigma,\ \theta|M_i)$ reflects the user's prior knowledge of the random field parameters in the absence of site-specific data. In this study, the four random field parameters, a, b, σ, and θ are assumed to be independently and uniformly distributed. In other words, the joint prior PDF of the random vector $[a,b,\sigma,\theta]$ is given by Eq. (8).

$$p(a,b,\sigma,\theta|M_i) = \frac{1}{(a_{\max}-a_{\min})(b_{\max}-b_{\min})(\sigma_{\max}-\sigma_{\min})(\theta_{\max}-\theta_{\min})} \text{ for } a\in[a_{\min},a_{\max}], b\in[b_{\min},b_{\max}], \sigma\in[\sigma_{\min},\sigma_{\max}], \theta\in[\theta_{\min},\theta_{\max}] \text{ and } 0 \text{ otherwise} \tag{8}$$

where $a_{\min}$, $b_{\min}$, $\sigma_{\min}$, and $\theta_{\min}$ are the minimum values of a, b, σ, and θ, respectively, and $a_{\max}$, $b_{\max}$, $\sigma_{\max}$, and $\theta_{\max}$ are the maximum values of a, b, σ, and θ, respectively. The values for the lower and upper bounds of the four random field parameters

could be determined based on the physical meaning of the parameters and users' experience. For example, the standard deviation and scale of fluctuation can only take positive values and their lower bounds could be set to small positive values such as 0.01. The evaluation of the evidence in Eq. (7) involves an integration of the product of the likelihood and prior PDF of random field parameters. When only a few random variables are involved, direct integration could be accomplished through some numerical integration techniques. For cases with many random variables, direct numerical integration of the evidence is computationally prohibitive and advanced techniques such as Markov Chain Monte Carlo simulation method can be resorted to (e.g. Wang and Cao, 2013; Tian et al., 2016). In this study, the direct numerical integration method is used because only four parameters are involved in the integration. To be specific, the range of each parameter is partitioned into a number of intervals and the evidence is the sum of the product of the integrand and the interval widths for each parameter as shown in Eq. (9).

$$P\left(\widehat{\mathbf{Y}}|M_i\right) \approx \sum_{j,k,l,m} p\left(\widehat{\mathbf{Y}}|a_j, b_k, \sigma_l, \theta_m\right) p(a_j, b_k, \sigma_l, \theta_m|M_i) \Delta a_j \Delta b_k \Delta \sigma_l \Delta \theta_m \tag{9}$$

where $p(\widehat{\mathbf{Y}}|a_j, b_k, \sigma_l, \theta_m)$ and $p(a_j, b_k, \sigma_l, \theta_m|M_i)$ respectively are the values of the likelihood function and prior PDF for $[a_j,\ b_k,\ \sigma_l,\ \theta_m]$, in which a_j, b_k, σ_l, and θ_m respectively are the median values of the jth interval of a, kth interval of b, lth interval of σ, and mth interval of θ; Δa_j, Δb_k, $\Delta \sigma_l$, and $\Delta \theta_m$ respectively are the width of jth interval of a, kth interval of b, lth interval of σ, and mth interval of θ. Note that a sufficient number of intervals are a prerequisite for an accurate evaluation of the integration. The number of intervals could be determined by parametric studies, i.e. by gradually increasing the number of intervals until a steady integration result is obtained.

3.2. Evaluation of posterior statistics of the random field model parameters using Bayesian updating method

The Bayesian updating method is well known to be able to consider the prior knowledge of geotechnical parameters and widely used in geotechnical engineering (e.g. Wang et al., 2010; Wang and Cao, 2013; Wang and Aladejare, 2016). In this study, the posterior knowledge (posterior mean and posterior standard deviation) of the random field model for UCS and EM is also determined using the Bayesian updating method. For this method, the posterior statistics can be obtained either by approximate solutions or by more advanced technique, such as Markov chain Monte Carlo simulation (e.g. Tian et al., 2016). The approximation method enables a fast evaluation of the posterior knowledge of random field parameters and is used in this study. The basic idea of the method is to approximate the posterior PDF with a Gaussian PDF with a mean vector equal to the most probable value (MPV) of the posterior PDF, $[a^*,\ b^*,\ \sigma^*, \theta^*]$ and covariance given by the inverse of a Hessian matrix, $\mathbf{H}(a^*, b^*, \sigma^*, \theta^*)$. The Hessian matrix is defined by the second-order derivation of an object function, $J(a,b,\sigma,\theta)$:

$$J(a, b, \sigma, \theta) = -\ln\left[p\left(\widehat{\mathbf{Y}}|a, b, \sigma, \theta; M_{\text{opt}}\right) p(a, b, \sigma, \theta|M_{\text{opt}})\right] \tag{10}$$

where M_{opt} is the selected optimal model. The (i, j) component of the Hessian matrix is given by Eq. (11).

$$H_{ij} = \frac{\partial^2}{\partial \omega_i \partial \omega_j} J(\omega)|_{\omega=\omega^*} \tag{11}$$

where $\omega = [\omega_1, \omega_2, \omega_3, \omega_4] = [a, b, \sigma, \theta]$ and $\omega^* = \left[a^*, b^*, \sigma^*, \theta^*\right]$. The most probable random field parameters could be obtained using an optimization method, such as *fminsearch* subroutine in the MATLAB platform while the Hessian matrix could be evaluated using a finite difference method. Note that for the Bayesian updating in this study, the prior distribution for each parameter is assumed to be a uniform distribution with an infinite distribution range. In other words, the parameter space for the regression coefficients is the semi-infinite plane which ensures a positive mean trend while the distribution ranges of standard deviation and scale of fluctuation are from 0 to positive infinity. These prior distributions are adopted because the prior information for the random field parameters is lacking. Details of the evaluation could be found in Wang et al. (2010), Yuen (2010a) and Cao and Wang (2013), and are not repeated herein.

4. Database of uniaxial compressive strength and elastic modulus for intact rocks

In this study, some uniaxial compressive strength and elastic modulus data for sedimentary and igneous rock are collected. The sedimentary rock data are from Singapore while the igneous rock data are from Sweden (download from http://www.skb.com/publications/). The rock type for the former is mainly sandstone. The rock samples for the latter are collected from the southeast of the Forsmark nuclear power plant, Sweden in 2002–2007 and the associated rock types are granite and diorite. Details of the UCS and EM data are plotted in Figs. 2 and 3. The data in each set in Figs. 2 and 3 are from the same borehole and belong to the same rock type. As shown in Figs. 2 and 3, 11 sets of data are available for both UCS and EM and the number of data points in each data set ranges from 10 to 21. As discussed in the introduction section, the rock data in practice are normally sparse because of the high cost of core drilling and sophistication of testing equipment. However, the Bayesian model class selection method is capable of dealing with limited data. As shown by Cao and Wang (2014), the Bayesian model class selection method could find out the right model even though the data are sparsely located. In the subsequent section, it is shown that the collected different sets of data have strikingly consistent autocorrelation models.

5. Results for selected autocorrelation model and updated random field parameters for UCS and EM

In this section, the selected most plausible autocorrelation models and associated posterior statistics of the random field parameters for the UCS and EM parameters are given. For the integration via Eq. (9), the integration regions with larger likelihood values (i.e. the region around the MPV of random field parameters) are partitioned into denser intervals. The whole integration space is divided into 1,000,000 parts, i.e. $n_a \times n_b \times n_\sigma \times n_\theta = 1{,}000{,}000$, where n_a, n_b, n_σ, and n_θ respectively are the numbers of intervals for a, b, σ and θ. This number ensures the convergence of the evidence. For example, the logarithms of the evidence for the SEACF model, $\ln[P(\widehat{Y}|M_1)]$, for 1,000,000 and 7,000,000 intervals respectively are −22.61 and −22.60, the difference between which is ignorable. In addition, for evaluating $P(\widehat{Y}|M_i)$, the prior ranges for the four parameters $[a,\ b,\ \sigma,\ \theta]$ of UCS are respectively set as $a \in \left[a_i^* - 2.5\ \text{MPa/m},\ a_i^* + 2.5\ \text{MPa/m}\right]$, $b \in \left[b_i^* - 250\ \text{MPa}, b_i^* + 250\ \text{MPa}\right]$, $\sigma \in [0.01\ \text{MPa}, 150\ \text{MPa}]$, and $\theta \in [0.01\ \text{m}, 50\ \text{m}]$, where a_i^* and b_i^* respectively are the most probable values of a and b when the autocorrelation model M_i is assumed. These bounds are wide enough to produce a correct solution of the most plausible model because the evidence does not change if wider prior ranges of $[a, b, \sigma, \theta]$ are

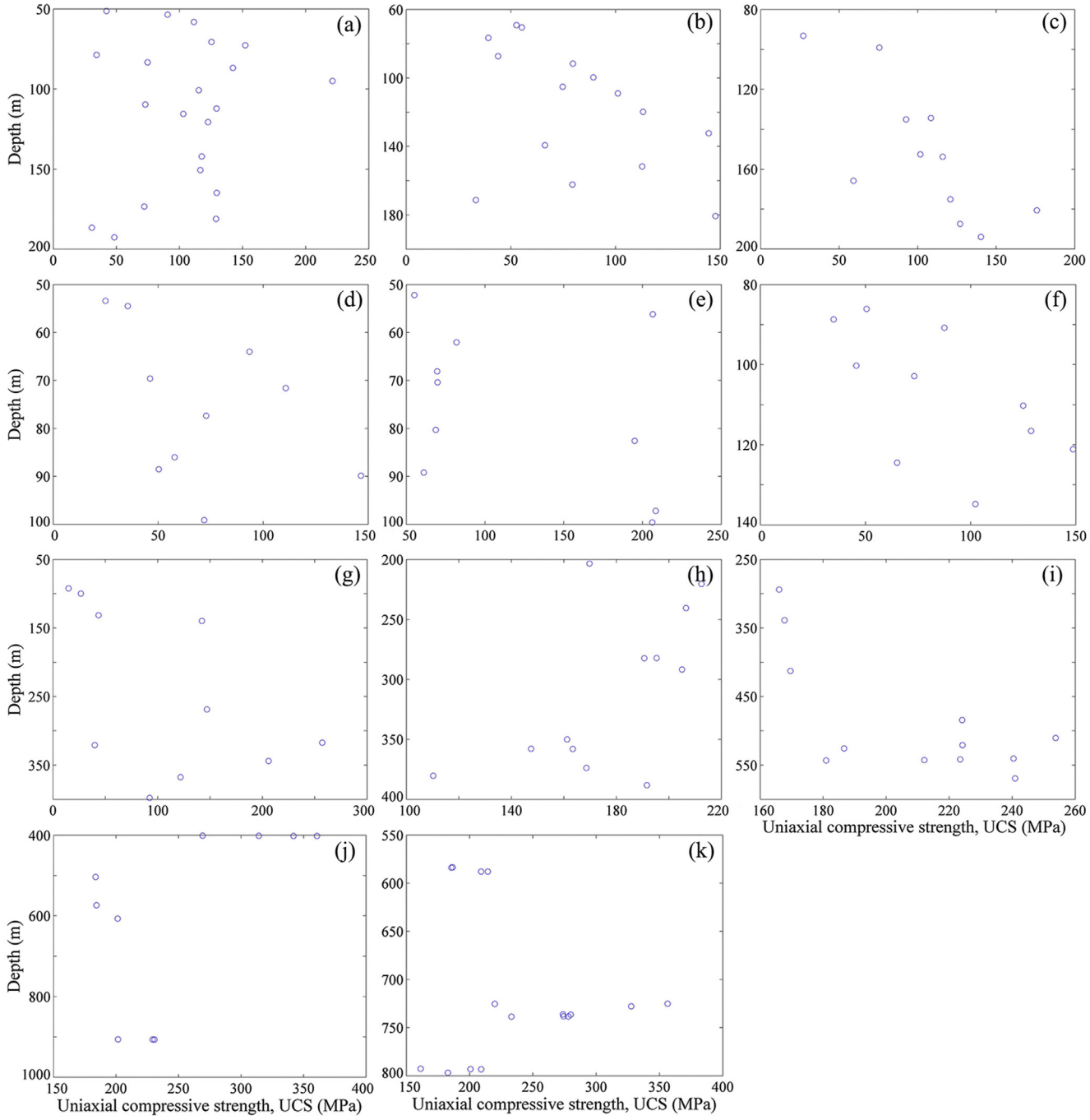

Figure 2. Collected uniaxial compressive strength data. (a) set 1 (sedimentary rock); (b) set 2 (sedimentary rock); (c) set 3 (sedimentary rock); (d) set 4 (sedimentary rock); (e) set 5 (sedimentary rock); (f) set 6 (sedimentary rock); (g) set 7 (sedimentary rock); (h) set 8 (igneous rock); (i) set 9 (igneous rock); (j) set 10 (igneous rock); (k) set 11 (igneous rock).

used, e.g. $[a_i^* - 5\ \text{MPa/m},\ a_i^* + 5\ \text{MPa/m}]$, $b \in \left[b_i^* - 500\,\text{MPa}, b_i^* + 500\ \text{MPa}\right]$, $\sigma \in [0.01\ \text{MPa}, 200\ \text{MPa}]$, and $\theta \in [0.01\ \text{m}, 100\ \text{m}]$. In addition, these ranges normally cover the 95% credible interval defined by the posterior statistics of the random field parameters, indicating that the selected prior ranges are wide enough to consider all the possible values of the random field parameters. Details of the credible interval are illustrated in section 5.2. Likewise, the prior ranges for the four parameters [a, b, σ, θ] of EM are respectively set as $a \in [a_i^* - 0.5\,\text{GPa/m}, a_i^* + 0.5\,\text{GPa/m}]$, $b \in \left[b_i^* - 50\ \text{GPa}, b_i^* + 50\,\text{GPa}\right]$, $\sigma \in [0.01\ \text{GPa}, 50\ \text{GPa}]$, and $\theta \in [0.01\ \text{m}, 100\ \text{m}]$.

5.1. Most plausible autocorrelation models for UCS and elastic modulus

The evidence for different autocorrelation models and different sets of UCS data is summarized in Table 1. As shown in Table 1, the single exponential autocorrelation function has the maximum values of evidence regardless of the rock type and data set, indicating the single exponential autocorrelation function is the most plausible model to describe the autocorrelation structure of the UCS of rocks. Table 2 summarizes the evidence for different autocorrelation models and different sets of elastic modulus data. As shown in Table 2, the exponential autocorrelation model also has

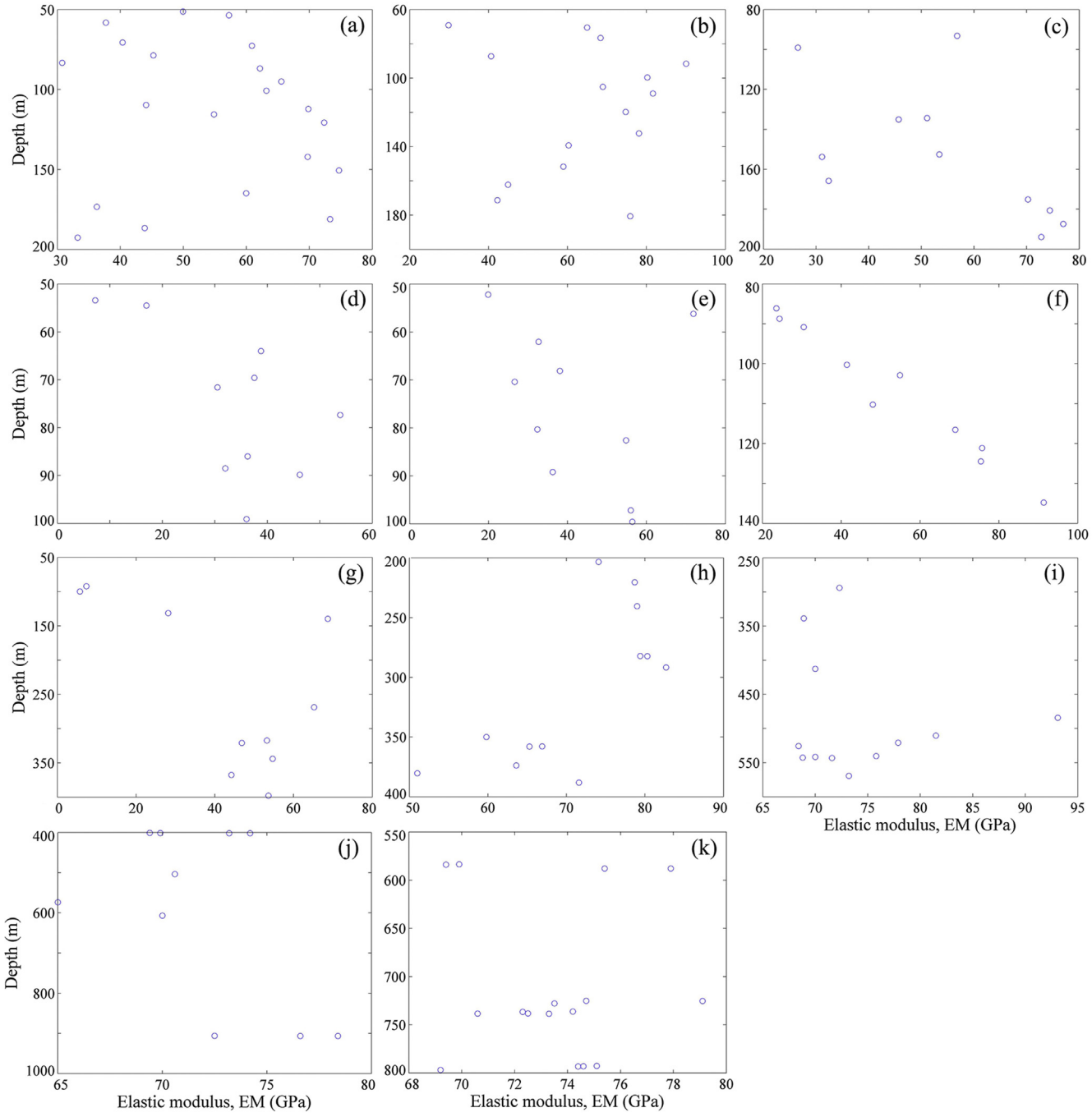

Figure 3. Collected elastic modulus data. (a) set 1 (sedimentary rock); (b) set 2 (sedimentary rock); (c) set 3 (sedimentary rock); (d) set 4 (sedimentary rock); (e) set 5 (sedimentary rock); (f) set 6 (sedimentary rock); (g) set 7 (sedimentary rock); (h) set 8 (igneous rock); (i) set 9 (igneous rock); (j) set 10 (igneous rock); (k) set 11 (igneous rock).

the maximum evidence in most cases. The astute readers may doubt the accuracy of the results because the collected UCS data are relatively limited (10–21 data points in each data set). However, as shown by Cao and Wang (2014), the Bayesian model class selection model could identify the most plausible model even when the sampling spacing is large. In addition, since all or most (10/11 = 91%) of the data sets have the same optimal autocorrelation function, it is of high confidence to conclude that the single exponential autocorrelation is the most suitable autocorrelation function for the UCS and elastic modulus of igneous and sedimentation rocks.

5.2. Posterior statistics of random field parameters

The posterior mean (μ_a^*, μ_b^*, μ_σ^* and μ_θ^*) and standard deviations (σ_a^{po}, σ_b^{po}, σ_σ^{po} and σ_θ^{po}) for the random field parameters of UCS are summarized in Table 3. When calculating the posterior standard deviations, some abnormal values such as extremely large values or infinity are obtained and denoted as "—" in Table 3. These abnormal values occur because certain diagonal component of the Hessian matrix is equal to or close to 0, resulting in a singular or nearly singular Hessian matrix. To further explore the reason, Fig. 4 plots the variation of the likelihood with the scale of fluctuation for set 3

Table 1
Logarithms of the evidence for different autocorrelation functions and different sets of UCS data.

		M1: Single exponential	M2: Gaussian	M3: Binary Noise	M4: Second-order Markov	M5: Cosine exponential
Sedimentary rock	Set 1	−22.61[a]	−23.59	−23.36	−23.21	−23.24
	Set 2	−14.40[a]	−15.12	−14.50	−14.72	−14.65
	Set 3	−8.34[a]	−9.48	−8.68	−9.05	−8.61
	Set 4	−13.09[a]	−13.99	−13.72	−13.76	−13.74
	Set 5	−12.83[a]	−13.31	−13.28	−13.19	−13.38
	Set 6	−10.70[a]	−12.00	−11.43	−11.70	−11.39
	Set 7	−18.16[a]	−18.36	−18.39	−18.31	−18.53
Igneous rock	Set 8	−1.57[a]	−3.44	−2.09	−3.02	−2.09
	Set 9	−0.66[a]	−2.52	−1.26	−1.98	−1.26
	Set 10	−1.85[a]	−6.73	−2.45	−4.83	−2.46
	Set 11	−7.32[a]	−9.19	−8.40	−8.82	−8.23

Note: [a] denotes the maximum value of the $\ln[P(\widehat{Y}|M_i)]$ for a set of UCS data.

Table 2
Logarithms of the evidence for different autocorrelation functions and different sets of EM data.

		M1: Single exponential	M2: Gaussian	M3: Binary Noise	M4: Second-order Markov	M5: Cosine exponential
Sedimentary rock	Set 1	−11.03[a]	−11.82	−11.78	−11.67	−11.81
	Set 2	−10.78[a]	−11.59	−11.46	−11.43	−11.50
	Set 3	−8.25[a]	−9.75	−9.02	−9.44	−9.02
	Set 4	−8.76[a]	−10.97	−9.49	−10.53	−9.46
	Set 5	−8.42[a]	−9.27	−9.05	−9.10	−9.09
	Set 6	1.92[a]	0.14	1.75	0.44	1.76
	Set 7	−9.37	−10.54	−9.32	−9.79	−9.24[a]
Igneous rock	Set 8	5.28[a]	3.47	4.85	3.91	4.89
	Set 9	5.72[a]	2.68	5.28	3.38	5.33
	Set 10	5.16[a]	1.49	4.53	2.04	4.54
	Set 11	17.94[a]	14.38	17.30	15.23	17.34

Note: [a] denotes the maximum value of the $\ln[P(\widehat{Y}|M_i)]$ for a set of EM data.

and set 7 of the UCS data. The likelihoods in Fig. 4 are calculated by setting the values of a, b and σ parameters to their MPVs, i.e. a^*, b^*, and σ^*, and altering the values of θ. As shown in Fig. 4, the likelihood may display different trends with the scale of fluctuation for different sets of data. For example, there is a peak of the likelihood around the MPV of the scale of fluctuation, θ^*, for the 3rd set of the UCS data. For this case, the second-order derivative of the objective function, $J(a,b,\sigma,\theta)$ is positive. However, for the 7th set of UCS data in Fig. 4b, the likelihood keeps constant around the θ^* and the second-order derivative of the objective function is 0 or nearly 0, resulting in infinite or very large posterior standard deviation of θ. In this case, the posterior PDF of the random field parameters cannot be approximated by a Gaussian distribution and the associated results are abandoned.

Excluding the abnormal data set in Table 3, it can be seen that the scale of fluctuation of UCS ranges from 0.3 m to 8 m and there is no apparent difference between the SoFs for sedimentary rocks and for igneous rocks. In addition, other useful information could also be deduced based on the posterior means and standard deviations of the random field parameters. For example, the posterior coefficient of variation (COV) of UCS at various depths are calculated by $\mathrm{COV}(z) = \sigma_\sigma^{\mathrm{po}}/\mu_{\mathrm{UCS}}^{\mathrm{po}} = \sigma_\sigma^{\mathrm{po}}/\left(\mu_a^* z + \mu_b^*\right)$, where $\sigma_\sigma^{\mathrm{po}}$ is the posterior standard deviation of σ, and $\mu_{\mathrm{UCS}}^{\mathrm{po}}$, μ_a^* and μ_b^* respectively are the posterior mean of UCS, a and b. Using this equation, it can be readily calculated that the COVs for various sets of UCS data ranges from 9% to 75%. The interval falls within the typical ranges provided by Aladejare and Wang (2017), which justify the analyses in this study. Apart from COV, the credible interval is another useful information in Bayesian statistics. The 95% credible interval of a parameter is a range within which the parameter falls with a probability of 95%. For a normally distributed random variable, the 95% mean value − centered credible interval is given by $[\mu^* - 1.96\sigma^{\mathrm{po}},\ \mu^* + 1.96\sigma^{\mathrm{po}}]$, where μ^* and σ^{po} respectively are the posterior mean and standard deviation of the parameter. For a lognormally distributed random variable, the 95% mean value−centered credible interval is given by $[\mu^*/\exp(1.96\sigma_N^{\mathrm{po}}),\ \mu^*\exp(1.96\sigma_N^{\mathrm{po}})]$, where $\sigma_N^{\mathrm{po}} = \sqrt{\ln(1+(\sigma^{\mathrm{po}}/\mu^*)^2)}$ is the posterior standard deviation for the logarithm of the parameter. Assuming the parameters a and b are normally distributed and σ and θ are lognormally distributed, it can be easily shown that the 95% credible intervals of a, b, σ and θ for the 1st set of UCS data respectively are [−0.45 MPa/m, 0.21 MPa/m], [71.50 MPa, 167.18 MPa], [34.9 MPa, 90.9 MPa] and [0.44 m, 26.26 m]. These intervals respectively fall within the prior range of a, b, σ and θ for evidence evaluations, i.e. $a \in [a_i^* - 2.5\,\mathrm{MPa/m}, a_i^* + 2.5\,\mathrm{MPa/m}] = [-2.62\,\mathrm{MPa/m}, 2.38\,\mathrm{MPa/m}]$, $b \in \left[b_i^* - 250\,\mathrm{MPa},\ \ b_i^* + 250\,\mathrm{MPa}\right] = [-130.66\,\mathrm{MPa}, 369.34\,\mathrm{MPa}]$, $\sigma \in [0.01\,\mathrm{MPa}, 150\,\mathrm{MPa}]$, and $\theta \in [0.01\,\mathrm{m}, 50\,\mathrm{m}]$. In other words, the prior ranges of a, b, σ and θ for evidence evaluations are large enough to consider all the possible values of these parameters. The credible intervals of random field parameters for other sets of UCS data still fall within the corresponding prior ranges and are not repeated herein.

The posterior statistics of random field parameters for the elastic modulus are summarized in Table 4. As shown in Table 4, the scale of fluctuation for elastic modulus ranges from 0.3 m to 8.4 m. Using the same method as that for the UCS, it can be easily deduced that the COV for the elastic modulus ranges from 4% to 88%. This range also accords with the results given by Aladejare and Wang (2017). The credible intervals for random field parameters of EM also fall within the corresponding prior ranges for evidence evaluations and are not repeated herein.

5.3. Differences of autocorrelation coefficient for different models

To illustrate the significance of autocorrelation function selection, Fig. 5 plots the autocorrelation coefficients for the optimal

Table 3
Posterior statistics for the random field parameters of UCS.

Rock type	Set number	Posterior MPV (or mean)				Posterior standard deviation			
		μ_a^* (MPa/m)	μ_b^* (MPa)	μ_σ^* (MPa)	μ_θ^* (m)	σ_a^{po} (MPa/m)	σ_b^{po} (MPa)	σ_σ^{po} (MPa)	σ_θ^{po} (m)
Sedimentary rock	Set 1	−0.12	119.34	56.31	3.40	0.17	24.41	13.95	4.77
	Set 2	0.09	75.28	39.85	8.02	0.24	30.89	11.83	9.18
	Set 3	0.86	−27.23	30.83	5.73	0.23	34.14	8.48	5.98
	Set 4	0.89	3.97	31.21	0.29	0.44	32.48	9.77	5.52
	Set 5	1.28	26.22	67.76	1.16	1.14	84.13	23.90	9.83
	Set 6	1.18	−39.92	32.42	0.13	0.48	50.59	9.45	—[a]
	Set 7	0.30	36.75	85.44	0.22	0.13	29.27	36.58	—[a]
Igneous rock	Set 8	−0.28	264.38	25.73	2.86	0.11	35.39	5.89	2.86
	Set 9	0.24	93.03	22.22	0.84	0.08	36.37	4.70	1.36
	Set 10	−0.07	268.74	50.39	4.14	0.13	78.20	15.81	3.36
	Set 11	0.03	214.20	54.24	0.52	0.16	113.77	12.38	0.50

Note: — [a] means abnormal values are obtained in Bayesian updating, such as extremely large values or infinity.

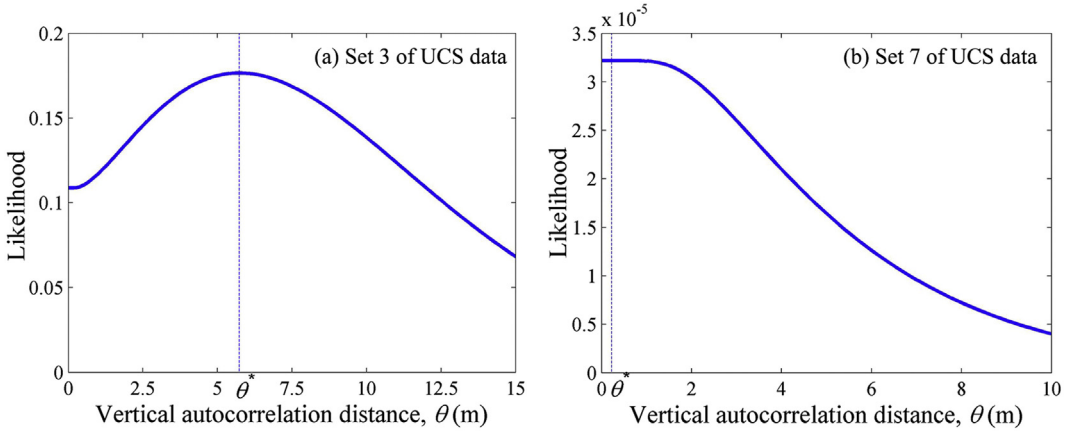

Figure 4. Variation of the likelihood with scale of fluctuation.

Table 4
Posterior statistics for the random field parameters of EM.

Rock type	Set number	Posterior MPV (or mean)				Posterior standard deviation			
		μ_a^* (GPa/m)	μ_b^* (GPa)	μ_σ^* (GPa)	μ_θ^* (m)	σ_a^{po} (GPa/m)	σ_b^{po} (GPa)	σ_σ^{po} (GPa)	σ_θ^{po} (m)
Sedimentary rock	Set 1	0.00	55.05	15.17	0.08	—[a]	—[a]	—[a]	—[a]
	Set 2	0.05	58.62	19.91	0.08	0.11	13.70	4.43	—[a]
	Set 3	0.31	7.40	16.58	0.85	0.15	23.06	4.65	6.92
	Set 4	0.64	−15.02	10.65	0.28	0.15	11.13	2.98	13.44
	Set 5	0.54	0.37	12.33	0.13	0.04	1.69	3.37	—[a]
	Set 6	1.40	−96.58	4.34	0.15	0.09	9.18	1.00	—[a]
	Set 7	0.16	1.51	14.29	1.50	0.03	6.43	4.34	2.14
Igneous rock	Set 8	−0.11	103.17	6.82	6.80	0.03	9.97	1.53	5.80
	Set 9	0.02	67.05	6.80	8.35	0.02	11.26	1.68	9.54
	Set 10	0.01	66.86	3.18	0.41	0.01	3.82	0.77	0.50
	Set 11	0.00	71.62	2.77	0.70	0.01	7.77	0.57	0.58

Note: — [a] means abnormal values are obtained in Bayesian updating, such as extremely large values or infinity.

autocorrelation model and other models with vertical separation distance. In Fig. 5a and b the autocorrelation coefficients for different models are plotted while in Fig. 5c and d the ratios of the autocorrelation coefficient for the non-optimal model to that for the optimal model are plotted. The autocorrelation coefficients for each model are calculated based on the MPVs of SoF. The MPVs of SoF for $M_1, M_2, \cdots, M_5$ respectively are 1.16 m, 0.69 m, 1.89 m, 1.75 m, and 2.28 m for the 5th set of UCS data while the MPVs are 4.139 m, 0.786 m, 2.144 m, 1.378 m and 2.215 m for the 10th set of UCS data. As shown in Fig. 5a and b, the autocorrelation coefficients for the single exponential model are quite different from other models. For example, the autocorrelation coefficients at $|\Delta z| = 2$ m for model M_1, M_2, $\cdots$, M_5 respectively are 0.38, 0, 0.07, 0.02, 0.25 in Fig. 5b. The differences are more evident in Fig. 5c and d. As shown in Fig. 5c, the autocorrelation coefficient for the cosine exponential autocorrelation function might be 12 times as large as that for the single exponential model. All these results highlight the significance of autocorrelation function model selection. It is worth noting that many studies evaluated the effect of autocorrelation functions (ACFs) on the reliabilities of geotechnical structures by assuming the same value of SoF for different ACFs (e.g. Li et al., 2015b; Liu et al., 2017c). This treatment is not reasonable because, based on the results of this study, different values of SoFs would be obtained for different ACFs if the same source of data is used.

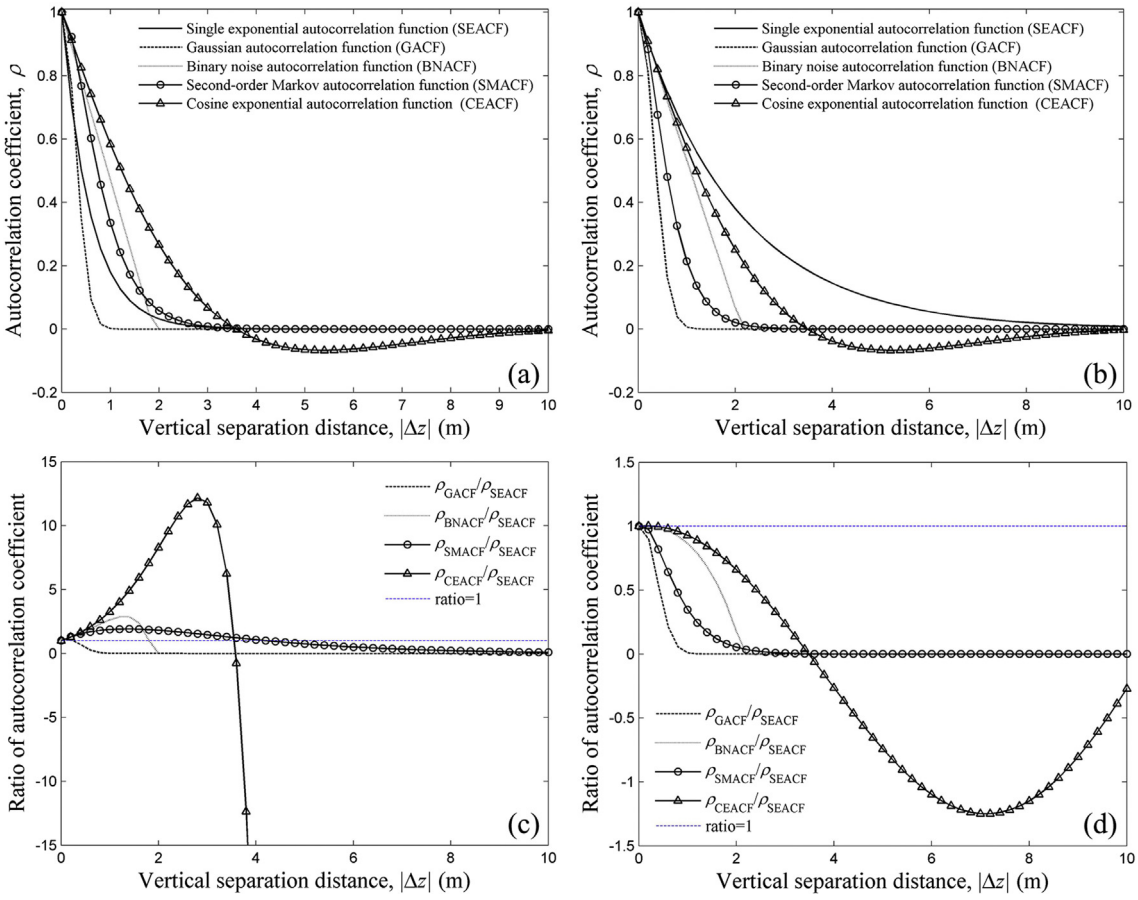

Figure 5. Differences between the autocorrelation coefficients for the optimal autocorrelation model and other models. (a) Autocorrelation coefficients for set 5 of UCS data; (b) autocorrelation coefficients for set 10 of UCS data; (c) ratio of autocorrelation coefficients for set 5 of UCS data; (d) ratio of autocorrelation coefficients for set 10 of UCS data.

6. Conclusions

In this paper, UCS and elastic modulus data for sedimentary and igneous rocks are collected. The autocorrelation structures are selected using a Bayesian model class selection approach and the posterior statistics of the scales of fluctuation for these two parameters are estimated using a Bayesian updating approach. The results show the autocorrelation structures for both UCS and EM could be best described by a single exponential autocorrelation function. The scales of fluctuation for UCS and EM respectively range from 0.3 m to 8.0 m and from 0.3 m to 8.4 m. The ranges of the scale of fluctuation are valid for rocks in similar geological environments and the same rock categories as studied in this paper. For other cases, the SoF ranges obtained in this paper could be applied as prior information and the scale of fluctuation could be updated using site specific data.

References

Aladejare, A.E., Wang, Y., 2017. Evaluation of rock property variability. Georisk: Assessment and Management of Risk for Engineered Systems and Geohazards 11 (1), 22–41.

Cao, Z., Wang, Y., 2013. Bayesian approach for probabilistic site characterization using cone penetration tests. Journal of Geotechnical and Geoenvironmental Engineering 139 (2), 267–276.

Cao, Z., Wang, Y., 2014. Bayesian model comparison and selection of spatial correlation functions for soil parameters. Structural Safety 49, 10–17.

Ching, J., Wu, S.S., Phoon, K.K., 2015. Statistical characterization of random field parameters using frequentist and Bayesian approaches. Canadian Geotechnical Journal 53 (2), 285–298.

Dasaka, S., Zhang, L., 2012. Spatial variability of in situ weathered soil. Géotechnique 62 (5), 375–384.

Gravanis, E., Pantelidis, L., Griffiths, D.V., 2014. An analytical solution in probabilistic rock slope stability assessment based on random fields. International Journal of Rock Mechanics and Mining Sciences 71, 19–24.

Goh, A.T.C., Zhang, Y., Zhang, R., Zhang, W., Xiao, Y., 2017. Evaluating stability of underground entry-type excavations using multivariate adaptive regression splines and logistic regression. Tunnelling and Underground Space Technology 70, 148–154.

Gong, W., Tien, Y.M., Juang, C.H., Martin, J.R., Luo, Z., 2017. Optimization of site investigation program for improved statistical characterization of geotechnical property based on random field theory. Bulletin of Engineering Geology and the Environment 76 (3), 1021–1035.

Hoek, E., Carranza-Torres, C., Corkum, B., 2002. Hoek-Brown failure criterion-2002 edition. In: Hammah, R. (Ed.), Mining and Tunnelling Innovation and Opportunity: Proceedings of the 5th North American Rock Mechanics Symposium and the 17th Tunnelling Association of Canada Conference, pp. 267–273. Toronto, Canada.

Hoek, E., Diederichs, M.S., 2006. Empirical estimation of rock mass modulus. International Journal of Rock Mechanics and Mining Sciences 43 (2), 203–215.

Hsu, S.C., Nelson, P.P., 2006. Material spatial variability and slope stability for weak rock masses. Journal of Geotechnical and Geoenvironmental Engineering 132 (2), 183–193.

Jaksa, M.B., Goldsworthy, J.S., Fenton, G.A., Kaggwa, W.S., Griffiths, D.V., Kuo, Y.L., et al., 2005. Towards reliable and effective site investigations. Géotechnique 55 (2), 109–121.

Li, H.Z., Low, B.K., 2010. Reliability analysis of circular tunnel under hydrostatic stress field. Computers and Geotechnics 37 (1–2), 50–58.

Li, D.Q., Qi, X.H., Phoon, K.K., Zhang, L.M., Zhou, C.B., 2014. Effect of spatially variable shear strength parameters with linearly increasing mean trend on reliability of infinite slopes. Structural Safety 49, 45–55.

Li, D.Q., Qi, X.H., Cao, Z.J., Tang, X.S., Zhou, W., Phoon, K.K., et al., 2015a. Reliability analysis of strip footing considering spatially variable undrained shear strength that linearly increases with depth. Soils and Foundations 55 (4), 866–880.

Li, D.Q., Jiang, S.H., Cao, Z.J., Zhou, W., Zhou, C.B., Zhang, L.M., 2015b. A multiple response-surface method for slope reliability analysis considering spatial variability of soil properties. Engineering Geology 187, 60–72.

Liu, H., Low, B.K., 2017. System reliability analysis of tunnels reinforced by rockbolts. Tunnelling and Underground Space Technology 65, 155–166.

Liu, Y., Lee, F.H., Quek, S.T., Beer, M., 2014. Modified linear estimation method for generating multi-dimensional multi-variate Gaussian field in modelling material properties. Probabilistic Engineering Mechanics 38, 42–53.
Liu, Y., Lee, F.H., Quek, S.T., Chen, E.J., Yi, J.T., 2015. Effect of spatial variation of strength and modulus on the lateral compression response of cement-admixed clay slab. Géotechnique 65 (10), 851–865.
Liu, Y., Jiang, Y.J., Xiao, H., Lee, F.H., 2017a. Determination of representative strength of deep cement-mixed clay from core strength data. Géotechnique 67 (4), 350–364.
Liu, Y., Hu, J., Wei, H., Saw, A.L., 2017b. A direct simulation algorithm for a class of beta random fields in modelling material properties. Computer Methods in Applied Mechanics and Engineering 326, 642–655.
Liu, L.L., Cheng, Y.M., Jiang, S.H., Zhang, S.H., Wang, X.M., Wu, Z.H., 2017c. Effects of spatial autocorrelation structure of permeability on seepage through anembankment on a soil foundation. Computers and Geotechnics 87, 62–75.
Lü, Q., Chan, C.L., Low, B.K., 2013. System reliability assessment for a rock tunnel with multiple failure modes. Rock Mechanics and Rock Engineering 46 (4), 821–833.
Lü, Q., Low, B.K., 2011. Probabilistic analysis of underground rock excavations using response surface method and SORM. Computers and Geotechnics 38 (8), 1008–1021.
Lü, Q., Sun, H.Y., Low, B.K., 2011. Reliability analysis of ground–support interaction in circular tunnels using the response surface method. International Journal of Rock Mechanics and Mining Sciences 48 (8), 1329–1343.
Phoon, K.K., Kulhawy, F.H., 1999. Characterization of geotechnical variability. Canadian Geotechnical Journal 36 (4), 612–624.
Phoon, K.K., Quek, S.T., An, P., 2003. Identification of statistically homogeneous soil layers using modified Bartlett statistics. Journal of Geotechnical and Geoenvironmental Engineering 129 (7), 649–659.
Phoon, K.K., Retief, J.V., 2016. Reliability of Geotechnical Structures in ISO2394. CRC Press, London, UK.
Tian, M., Li, D.Q., Cao, Z.J., Phoon, K.K., Wang, Y., 2016. Bayesian identification of random field model using indirect test data. Engineering Geology 210, 197–211.
Wang, Y., Aladejare, A.E., 2015. Selection of site-specific regression model for characterization of uniaxial compressive strength of rock. International Journal of Rock Mechanics and Mining Sciences 75, 73–81.
Wang, Y., Aladejare, A.E., 2016. Evaluating variability and uncertainty of geological strength index at a specific site. Rock Mechanics and Rock Engineering 49 (9), 3559–3573.
Wang, Y., Au, S.K., Cao, Z., 2010. Bayesian approach for probabilistic characterization of sand friction angles. Engineering Geology 114 (3), 354–363.
Wang, Y., Cao, Z., 2013. Probabilistic characterization of Young's modulus of soil using equivalent samples. Engineering Geology 159, 106–118.
Yuen, K.V., 2010a. Bayesian Methods for Structural Dynamics and Civil Engineering. John Wiley & Sons, Singapore. Chapter 6.
Yuen, K.V., 2010b. Recent developments of Bayesian model class selection and applications in civil engineering. Structural Safety 32 (5), 338–346.
Zhang, W.G., Goh, A.T.C., 2013. Multivariate adaptive regression splines for analysis of geotechnical engineering systems. Computers and Geotechnics 48, 82–95.
Zhang, W.G., Goh, A.T.C., 2014. Multivariate adaptive regression splines model for reliability assessment of serviceability limit state of twin caverns. Geomechanics and Engineering 7 (4), 431–458.
Zhang, W.G., Goh, A.T.C., 2016. Multivariate adaptive regression splines and neural network models for prediction of pile drivability. Geoscience Frontiers 7 (1), 45–52.
Zhu, H., Zhang, L.M., 2013. Characterizing geotechnical anisotropic spatial variations using random field theory. Canadian Geotechnical Journal 50 (7), 723–734.